Hyperfine Structure of ^{67}Ga and ^{72}Ga*

Vernon J. Ehlers,† Yurdanur Kabasakal,‡ Howard A. Shugart, and Orhan Tezer‡

Lawrence Radiation Laboratory and Department of Physics, University of California, Berkeley, California

(Received 11 April 1968)

We have used the atomic-beam magnetic-resonance technique to measure the hyperfine-structure separations and the differential hyperfine-structure anomalies of 78-hour ^{67}Ga and 14-hour ^{72}Ga in the $^2P_{3/2}$ and $^2P_{1/2}$ electronic states. From the differential hyperfine-structure anomaly we have deduced the standard hyperfine-structure anomaly for the two J states. We have also calculated the nuclear moments from the measured hyperfine-structure separations. Our results are, for ^{67}Ga ($I=\frac{3}{2}$): $\Delta\nu(^2P_{1/2}) = 2457.727\,26(90)$ MHz, $a(^2P_{3/2}) = 175.097\,36(15)$ MHz, $b(^2P_{3/2}) = 71.957\,50(55)$ MHz, $^{67}\delta^{69} = 2.51(13)\times10^{-5}$, $^{67}\Delta^{69}(^2P_{1/2}) = 5.0(1.4)\times10^{-6}$, $^{67}\Delta^{69}(^2P_{3/2}) = -20.1(2.0)\times10^{-6}$, μ_I(uncorr) $= +1.8454(3)\mu_N$, and $Q = +0.22$ b; and for ^{72}Ga($I=3$): $\Delta\nu(^2P_{1/2}) = -153.652\,66(53)$ MHz, $a(^2P_{3/2}) = -6.256\,98(11)$ MHz, $b(^2P_{3/2}) = 193.673\,65(80)$ MHz, $^{71}\delta^{72} = 2.12(18)\times10^{-4}$, $^{71}\Delta^{72}(^2P_{1/2}) = 4.2(1.2)\times10^{-5}$, $^{71}\Delta^{72}(^2P_{3/2}) = -17.0(2.0)\times10^{-5}$, μ_I (uncorr) $= -0.131\,86(2)\mu_N$, $Q = +0.59$ b. The quoted values of the nuclear magnetic moments include a correction for the hyperfine-structure anomaly, but do not include the diamagnetic correction.

I. INTRODUCTION

Historically, gallium has been an important and frequent subject of atomic-beam studies. Because gallium is readily detected by ionization on a hot oxidized tungsten wire, its stable isotopes are particularly amenable to study with the atomic-beam technique. Also, the metastable $^2P_{3/2}$ state is well populated by thermal excitation at the temperatures required to produce a beam of gallium atoms; the presence of two electronic states in the beam allows performance of interesting experiments. As an example, measurement of the electronic g factors of the two electronic states of gallium permitted the first determination of the anomalous electron magnetic moment.[1]

Another interesting parameter which may be determined by study of the hyperfine structure of two electronic states is the differential hyperfine-structure anomaly.[2-4] The hfs anomaly is very small in a $^2P_{1/2}$ or $^2P_{3/2}$ state, and thus an extremely accurate measurement of the nuclear magnetic moments is normally required in order to determine this anomaly. Because such accurate measurements of nuclear magnetic moments are very difficult for radioactive isotopes in P electronic states, hfs anomalies which rely on this measurement are not easily determined. However, by measuring the hyperfine structure in two electronic states, one can determine the differential hyperfine-structure anomaly; from this one may deduce the standard hfs anomaly.[5] The value of the anomaly thus obtained can then be used to calculate the nuclear magnetic moment, from the observed hfs separations, with great accuracy. Additionally, the hyperfine-structure anomaly is itself of intrinsic interest, as it provides information about the internal structure of the nucleus.

Because the hyperfine structure of the stable gallium isotopes has previously been determined with high precision,[6,7] and because ^{67}Ga and ^{72}Ga have convenient half-lives which allow performance of precision experiments on these radioactive isotopes, we decided to investigate the hyperfine structure of these two isotopes with a view to measuring the hfs anomalies and nuclear moments to high precision.

II. GENERAL PRINCIPLES

A. The Hyperfine-Structure Interaction

The hyperfine structure Hamiltonian for an atom of nuclear spin I and electronic spin J in an external magnetic field is given by

$$\mathcal{H} = a\vec{I}\cdot\vec{J} + b\frac{3(\vec{I}\cdot\vec{J})^2 + \frac{3}{2}(\vec{I}\cdot\vec{J}) - I(I+1)J(J+1)}{2I(2I-1)J(2J-1)} + c\,\mathcal{O}_{op} - g_J(\mu_0/h)\vec{J}\cdot\vec{H} - g_I(\mu_0/h)\vec{I}\cdot\vec{H} \qquad (1)$$

where a, b, and c are the magnetic dipole, electric quadrupole, and magnetic octupole interaction constants, $g_J = \mu_J/J$ and $g_I = \mu_I/I$ are the electronic and nuclear g factors expressed in Bohr magnetons, and $\mathcal{O}_{op}$ is given by

$$\mathcal{O}_{op} = \{10(\vec{I}\cdot\vec{J})^3 + 20(\vec{I}\cdot\vec{J})^2 + 2(\vec{I}\cdot\vec{J})[-3I(I+1)J(J+1) + I(I+1) + J(J+1) + 3] - 4I(I+1)J(J+1)\} \times [I(I-1)(2I-1)J(J-1)(2J-1)]^{-1}. \qquad (2)$$

The magnetic octupole interaction constant c turned out to be zero within the accuracy of this experiment, and thus we will drop this term from our discussion. For the case $J=\frac{1}{2}$, the quadrupole and octupole terms drop out, and the remaining Hamiltonian may be solved analytically to obtain a closed expression for the energy as a function of magnetic field.[8] For the case $J=\frac{3}{2}$, the problem is most readily solved by numerically diagonalizing

the Hamiltonian matrix with the aid of a computer. The energy levels as a function of magnetic field are generally plotted as the familiar Breit-Rabi diagram; such a diagram for the $^2P_{3/2}$ state of ^{67}Ga is shown in Fig. 1.

The interaction constants a and b are proportional to the magnetic dipole and electric quadrupole nuclear moments, respectively. The relationships between these interaction constants and their associated nuclear moments, for the case of one electron outside closed shells, are well known and are given by the following formulas[9]:

$$a = 2g_I \mu_0 [L(L+1)/J(J+1)] \langle 1/r^3 \rangle_{\rm av} \mathcal{F} , \quad (3)$$

$$b = e^2 Q [2L/(2L+3)] \langle 1/r^3 \rangle_{\rm av} \mathcal{R} , \quad (4)$$

where μ_0 is the Bohr magneton, Q is the nuclear electric quadrupole moment, $\mathcal{F}$ and $\mathcal{R}$ are relativistic corrections given by Casimir,[10] L is the orbital angular momentum of the electron outside the closed shells, and the average value is taken with respect to this electron's wave function.

Ideally, one would wish to use these formulas to obtain values for μ_I and Q after measurement of a and b. The problem in this procedure lies in the calculation of $\langle 1/r^3 \rangle_{\rm av}$. Evaluation of this quantity depends upon a detailed knowledge of the wave function of the outer electron, and this in general is not well known. There are additional complications arising from configuration interaction; these factors have been considered for Ga by Koster,[9] who lists correction terms for Eqs. (3) and (4). However, for the assumption of a point nucleus, the quantity $\langle 1/r^3 \rangle_{\rm av}$ should be a constant for the various isotopes of a particular element. Thus, if we take the ratio of Eq. (3) for isotopes 1 and 2 of an element, and do the same for Eq. (4), we obtain the familiar Fermi-Segrè equations,

$$a_1/a_2 = g_{I_1}/g_{I_{22}} . \quad (5)$$

$$b_1/b_2 = Q_1/Q_2 . \quad (6)$$

We note from Eqs. (5) and (6) that if the nuclear moments and hfs have been determined for a particular isotope, then within the accuracy of the equation one can readily determine the nuclear moments of another isotope of that element merely by measuring the hfs interaction constants a and b. This is the technique normally used to determine the nuclear moments of radioactive isotopes, where direct measurements of nuclear moments are very difficult.

B. The Hyperfine-Structure Anomaly

Although Eqs. (5) and (6) are valid to rather high accuracy, deviations from Eq. (5) have been observed. These deviations are collectively termed the hfs anomaly, defined by[11]

$$^1\Delta^2 = (a_1/a_2)(g_{I_2}/g_{I_1}) - 1 . \quad (7)$$

The hfs anomaly arises simply because the nucleus is not a point, but has finite extent and structure. Contributions to the hfs anomaly are primarily due to two causes: (a) a difference in the distribution of nuclear magnetism in the two isotopes (Bohr-Weisskopf effect),[11] and (b) a difference of charge distribution in the two nuclei (Breit-Rosenthal effect).[12] These have been examined in detail by several authors.[13] Because these hfs anomalies can become quite large, care must be exercised in calculating nuclear moments from hfs interaction constants.

In the case of gallium, which has a single p electron outside closed shells, one expects an extremely small hfs anomaly, due to the very small value of the p-electron wave function at the nucleus. However, Schwartz has shown that there is a significant admixture of the s-electron wave function in the $^2P_{1/2}$ and $^2P_{3/2}$ states of gallium, and thus the hfs anomaly is larger than expected.[5] Additionally, the $^2P_{3/2}$ anomaly is three times as large as the $^2P_{1/2}$ anomaly, contrary to what one would normally expect.

We note that if we write Eq. (7) for two different electronic states, $J = \frac{1}{2}$ and $J = \frac{3}{2}$, and divide one equation by the other, we obtain

$$\left(\frac{a_1}{a_2}\right)_{1/2}\left(\frac{a_2}{a_1}\right)_{3/2} = \frac{1 + {}^1\Delta^2_{1/2}}{1 + {}^1\Delta^2_{1/2}} \approx 1 + {}^1\Delta^2_{1/2} - {}^1\Delta^2_{3/2} , \quad (8)$$

where we have assumed

$$\left(g_{I_1}/g_{I_2}\right)_{1/2} = \left(g_{I_1}/g_{I_2}\right)_{3/2} \quad (9)$$

and have neglected second-order terms in Δ.

If we now define the differential hfs anomaly $^1\delta^2$ as

$$^1\delta^2 = {}^1\Delta^2_{1/2} - {}^1\Delta^2_{3/2} = \left(\frac{a_1}{a_2}\right)_{1/2}\left(\frac{a_2}{a_1}\right)_{3/2} - 1, \quad (10)$$

we note that we can obtain the differential hfs

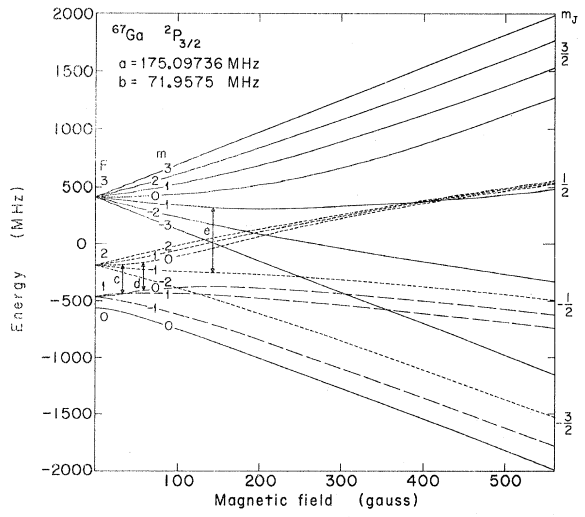

FIG. 1. The Breit-Rabi diagram for ^{67}Ga in the $^2P_{3/2}$ electronic state. (A similar figure for ^{72}Ga, showing its inverted level structure, is displayed in Ref. 15.)

anomaly simply by measuring the magnetic dipole interaction constant a for two different isotopes in two electronic states. Furthermore, we expect the ratio of the two hfs anomalies in the two electronic states to be a constant for all isotopes of an element, as this ratio depends only on atomic properties and has little dependence upon nuclear effects.[5] Because this ratio has already been measured for ^{69}Ga and ^{72}Ga, we can use this to obtain the actual hfs anomalies for radioactive isotopes for which the differential hfs anomaly has been measured.

III. EXPERIMENTAL DETAILS

A. Isotope Production and Preparation

^{72}Ga is easily produced by neutron bombardment of natural gallium, with the (n,γ) reaction on ^{71}Ga yielding substantial amounts of ^{72}Ga; the irradiated material could be placed without further preparation directly into the oven in our atomic-beam apparatus. The only difficulty in the handling of this isotope resulted from its high decay energy. This caused dangerously high levels of radiation from samples of any appreciable size, and required extensive shielding around the atomic-beam apparatus.

The ^{67}Ga was produced from ^{65}Cu by an $(\alpha, 2n)$ reaction, using first the 60-in. (152.4-cm) Crocker cyclotron, and later the 88-in. (223.5-cm) cyclotron. Bombardments of 400 μA hours typically provided sufficient material for a 5-hour run. The gallium was chemically separated from the Cu target material by the diethyl-ether extraction of $GaCl_3$ from a 6N HCl solution. The copper target was first dissolved in 10N HNO_3, which also contained about 20 mg of gallium carrier. After drying, the material was redissolved in 6N HCl and the ether extraction was then performed. The $GaCl_3$ was extracted from the ether with H_2O, and NaOH was added until a pH of 5.5 was achieved; at this point the Ga precipitates as $Ga(OH)_3$. The precipitate was redissolved in 10N NaOH, and the Ga was then electroplated onto a short length of platinum wire. Separation efficiencies of 85–90% were commonly obtained.

B. Radio-Frequency Equipment

Because we were attempting a precision measurement of the hfs, it was essential that the radio-frequency-generating equipment be extremely stable and accurate. All radio-frequency equipment was phase-locked to an external James Knight 100-kHz quartz-crystal frequency standard, which was in turn compared periodically with an Atomichron and the WWVB frequencies. A Schomandl FD3 frequency synthesizer was used to generate frequencies in the range 300–1000 MHz, whereas a Schomandl ND5 + NDF2 frequency synthesizer provided frequencies below 300 MHz. Frequencies above 1000 MHz were obtained by crystal multiplication and amplification of the FD3 output. Radio-frequency amplification was achieved by use of a Boonton model 230A amplifier (0–500 MHz), an Applied Microwave Laboratories amplifier (500–2000 MHz), and traveling-wave-tube amplifiers (above 2000 MHz). Frequencies were counted by use of Hewlett-Packard 5245L frequency counters and appropriate frequency-converter plug-in units.

C. Hairpins

The application of radio-frequency fields to an atomic beam involves several difficulties; the problems become particularly acute when one is performing precision measurements. It is desirable to have an rf field uniform in both phase and amplitude along the entire length of the region of interaction with the beam of atoms. For precision measurements, the interaction region should be as long as possible in order to have a narrow (uncertainty principle) width for the resonance line. However, as the length of the interaction region increases, generation of a homogeneous rf field becomes more difficult. This difficulty can be avoided by use of the Ramsey separated-oscillating-field technique,[14] but then difficulties are encountered (a) in identifying the central peak or minimum of the resonance pattern, and (b) in insuring that the rf field in the two hairpins is either precisely in or precisely out of phase. Although this presents no great problem in measurements on stable isotopes, where the entire resonance pattern may be readily examined at a glance, the difficulties of doing this for radioactive atomic-beam work often outweigh the advantages of this particular technique.

In an attempt to overcome these problems, we designed the hairpin illustrated schematically in Fig. 2. It is of a simple box-type construction, with a long center conductor shorted at the bottom of the hairpin. During construction, care was taken to keep all surfaces as parallel as possible; these surfaces were also polished and silver-plated. The magnetic field lines in this hairpin consist of elongated ovals around the center conductor. Because the static magnetic field is perpendicular to the length of the hairpin, the rf field at the two ends of the hairpins will be in the direction of the magnetic field, while the rf field in the

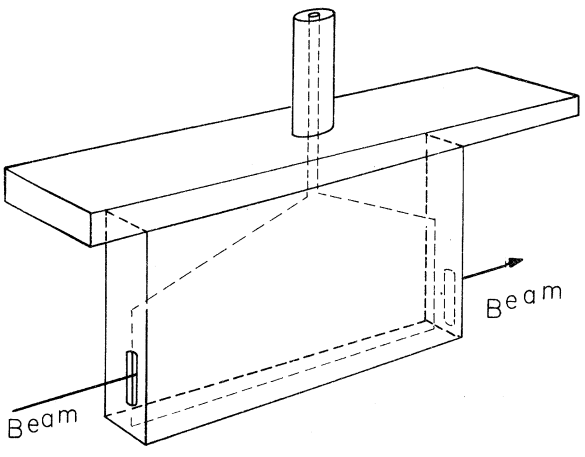

FIG. 2. A schematic drawing showing the type of hairpin used in this experiment.

center of the hairpin will be perpendicular to the static field. Thus the long central rf field will induce $\Delta m = 1$ transitions, and the end rf field will induce $\Delta m = 0$ transitions. Because the two end fields are exactly 180 deg out of phase, they will result (for $\Delta m = 0$ transitions) in a Ramsey pattern with a central minimum.

This type of hairpin was constructed in two lengths, 3 in. (7.6 cm) and 6 in.(15.2 cm). Before it was used upon the radioactive gallium isotopes, it was thoroughly tested with stable alkali atoms (see Appendix, subsection A). In all respects the hairpins behaved better than one would expect for such a simple design. The 3-in. hairpin gave consistent and accurate results with both the potassium and rubidium, but the 6-in. hairpin exhibited structure effects in looking at the (≈3000 MHz) transitions in rubidium.

We were particularly concerned about the possibility that the end fields were not exactly 180 deg out of phase, and that there might be a phase difference which would result in a nonsymmetric resonance. The $\Delta m = 0$ transitions were examined carefully, and no evidence for a phase shift was found. The Ramsey patterns observed in ^{39}K with the 3-in. and 6-in. hairpins, are shown in Fig. 3, where they are compared with a similar pattern obtained with the $\frac{5}{8}$-in. (1.6 cm) rigid-coaxial-line type of hairpin normally used in our work.

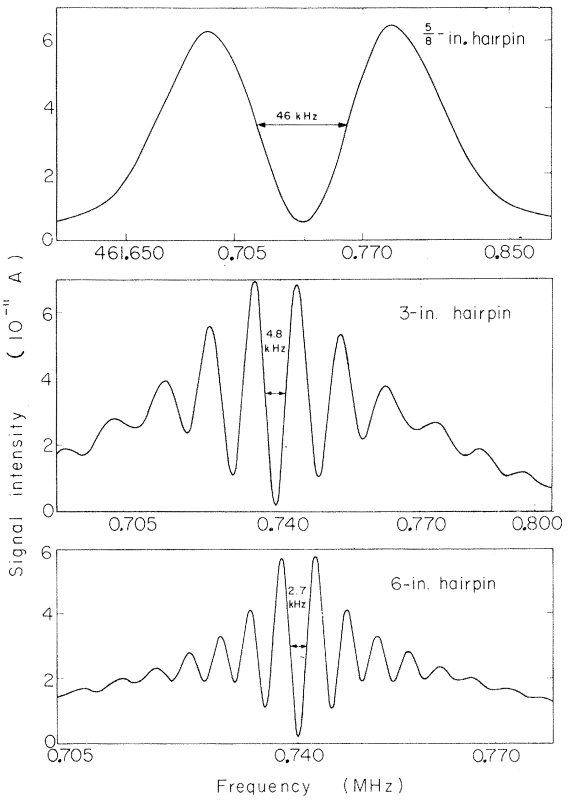

FIG. 3. Ramsey patterns obtained by sweeping the ^{39}K (2.0) ⟷ (1,0) transition with 3-inch and 6-inch hairpins of the type shown in Fig. 2, and a $\frac{5}{8}$-inch rigid-coaxial-line hairpin. Note the increasingly narrow maxima and minima as the hairpin length is increased.

We were also concerned about shifts of resonance lines caused by overpowering. Thus, a careful study was made of the ^{39}K and ^{85}Rb resonances as a function of rf power; the results of this investigation are also shown in the Appendix, subsection A. Typically, the $\Delta m = 1$ lines would optimize at an rf power of approximately 15 mW while the $\Delta m = 0$ lines usually required about 300 mW, with the 6-in. hairpin. The relative magnitudes of these optimization powers are an indication of the relative lengths of the rf fields inducing these transitions. As the rf field is increased, while one has the frequency set on top of a resonance, the height of the resonance will pass through several maxima and minima. This behavior, as observed with the 6-in. hairpin, is illustrated in Fig. 4 for a $\Delta m = 1$ transition. Because of the danger of distorting resonances by application of too much rf power, a curve similar to Fig. 4 was obtained for each resonance observed in the radioactive gallium isotopes.

D. Experimental Procedure

The atomic-beam apparatus used in this experiment was of conventional flop-in design. The homogeneous magnetic field was provided by a Varian 12-in. (30.5 cm) electromagnet. Field inhomogeneities were small enough so that no line broadening was observed, even with the 6-in. hairpin, for the field-independent gallium transitions measured in this experiment.

The beam of gallium atoms was obtained by heating gallium metal in a graphite oven with a 0.005-in. (0.13 mm) slit. The atoms transmitted through the beam apparatus were detected by collecting them on a sulphur-coated button, which was then counted in Geiger counters or NaI crystal counters for ^{72}Ga and ^{67}Ga, respectively. The crystal counters were set to observe the 90-keV gamma ray emitted in the decay of ^{67}Ga, and thus discriminated against any other activity present in the sample.

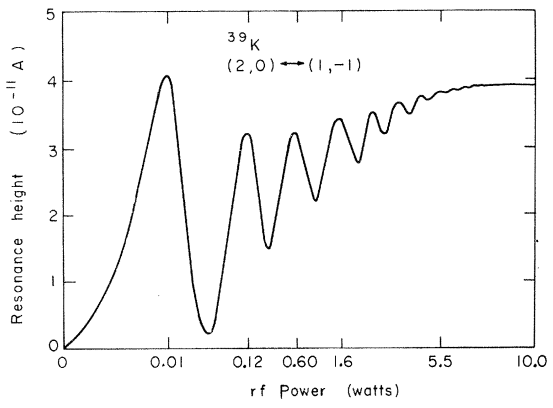

FIG. 4. A trace of the height of the ^{39}K (2,0) ⟷ (1, −1) transition as a function of radio-frequency power. The frequency was held constant at 445.9783 MHz and the field was 44.14 G. The hairpin had a 6-inch length. Note the nonlinear abscissa.

Two beam normalization methods were employed. In the earlier runs, the beam intensity was monitored before and after each rf-on exposure, by collecting a sample of the beam with the stop wire removed. In the later runs, two sample collectors were placed side by side at the detector position. The central button could collect only atoms which had undergone an rf transition, while the button placed alongside it collected atoms on the Stern-Gerlach peak, i.e., atoms which had not undergone a transition. The side button therefore provided a good measure of the integrated beam intensity during the entire exposure of the center button. The ratio of the counting rates of the two buttons then provided a normalized measure of the number of atoms undergoing transitions.

All transitions were observed at their field-independent points in order to minimize any effects caused by inhomogeneity of the static magnetic field. A list of the transitions observed is given in Table I, which also lists the field at which the transition is field-independent, and the frequency at that field. Figure 5 shows the behavior of most of the observed lines as a function of magnetic field; the field-independent points occur at the minima of the curves. The field was stabilized with a NMR field-locking device to prevent drift of the magnetic field during the course of a run.

Because the hfs constants of ^{67}Ga and ^{72}Ga have previously been determined to reasonably high accuracy,[15,2,16] many of the normal search problems were avoided. The procedure we followed was to calculate where a particular resonance should lie, based on the earlier work, and then to conduct a frequency sweep over that area. The power used for this initial sweep was calculated from the optimum power required to induce a transition in the calibration isotope at the same frequency, taking into consideration the relative transition probabilities for the two transitions (the method of calculating these transition probabilities is given in the Appendix, subsection B). After the peak of the resonance was established by this initial search, a study was made of the height of this resonance as a function of rf power. A typical result is shown in Fig. 6. Based on this result, an-

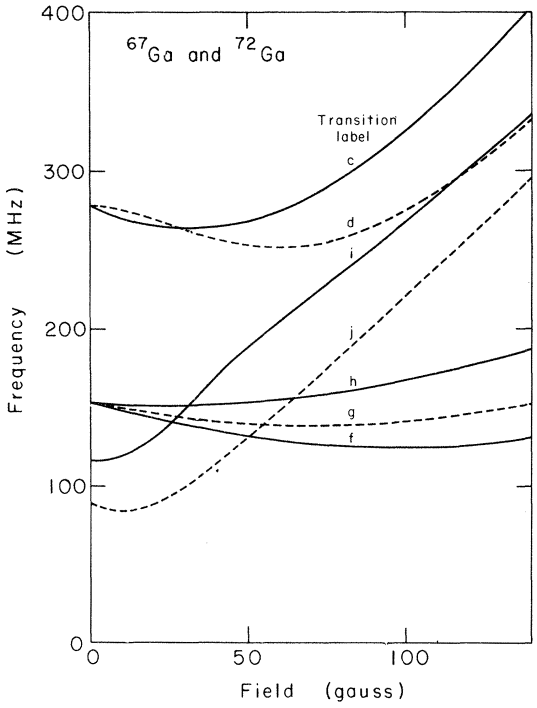

FIG. 5. Frequency as a function of magnetic field for several ^{67}Ga and ^{72}Ga transitions. The transition labels are explained in Table I.

TABLE I. Field-independent points of transitions in ^{67}Ga and ^{72}Ga.

Isotope	Electronic state	Transition label	F_1	m_1	F_2	m_2	Field (G)	Frequency (MHz)
^{67}Ga	$^2P_{1/2}$	*a*	2	0	1	0	0	2457.727
		b	2	0	1	−1	708.69	2373.322
	$^2P_{3/2}$	*c*	2	0	1	1	31.47	263.608
		d	2	0	1	0	60.09	252.049
		e	3	−1	2	−1	143.19	575.752
^{72}Ga	$^2P_{1/2}$	*f*	5/2	5/2	7/2	3/2	97.22	125.124
		g	5/2	3/2	7/2	3/2	70.67	138.826
		h	5/2	1/2	7/2	1/2	23.56	152.077
	$^2P_{3/2}$	*i*	9/2	3/2	7/2	5/2	1.98	116.921
		j	5/2	5/2	7/2	5/2	9.98	84.803

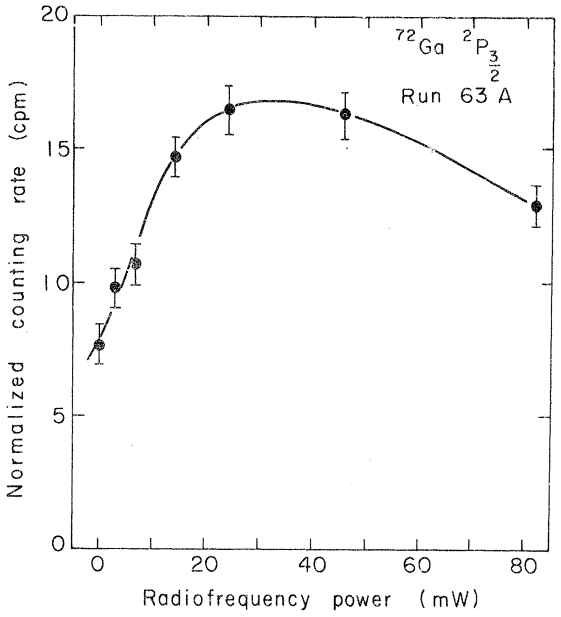

FIG. 6. The height of the ^{72}Ga $^2P_{3/2}$ (9/2, 3/2) ⟷ (7/2, 5/2) transition as a function of radio-frequency power. The frequency put into the 6-inch hairpin was held constant at 116.921 MHz. H=1.9 G.

other sweep was made with an rf power of approximately 70% of the optimum rf power. A typical resonance obtained with the 6-in. hairpin on a $\Delta m = 1$ transition is shown in Fig. 7. A similar resonance obtained with the 3-in. hairpin at a high frequency is displayed in Fig. 8, and displays the

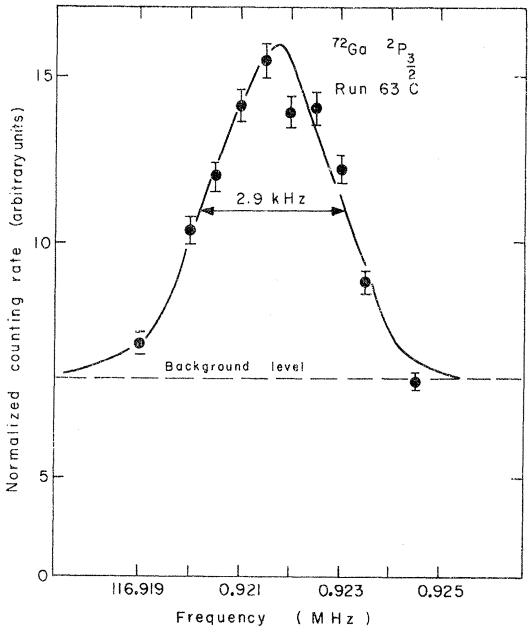

FIG. 7. A resonance corresponding to the ^{72}Ga $^2P_{3/2}$ (9/2, 3/2) ⟷ (7/2, 5/2) transition at 1.9 G, observed with the 6-inch hairpin.

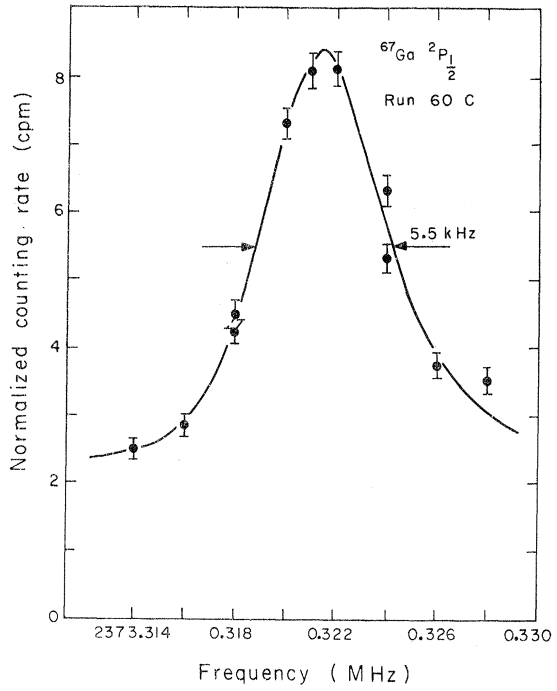

FIG. 8. A resonance corresponding to the ^{67}Ga $^2P_{1/2}$ (2,0) ⟷ (1,−1) transition observed at a field of 708.7 with the 3-inch hairpin. If there were no perturbation of the $^2P_{1/2}$ state by the $^2P_{3/2}$ state (Clendenin effect), the resonance would lie approximately 3 kHz higher.

quality of resonances obtained with this hairpin even at such extreme frequencies.

Observations of $\Delta m = 0$ transitions posed quite different problems. The major problem arose from the Ramsey pattern obtained for this case. Although it is quite easy to locate the central minimum when observing a stable isotope, both by virtue of its position and because the central minimum is the lowest minimum in the curve (and indeed is at background level), it is more difficult to observe this with a radioactive material. One can, of course, trace out the complete resonance, taking many points; this brute-force method was used on one of the ^{72}Ga lines to make a positive identification of the central minimum. The result of this extensive sweep is displayed in Fig. 9. However, this is not an ideal approach, as it is extremely time-consuming and wasteful of material. Although the latter consideration did not affect our work on ^{72}Ga, where there was no shortage of material, it became of prime importance in the measurement of ^{67}Ga, where only limited amounts were available. Thus a new search procedure was established. It can be best understood by referring to Fig. 3, where we note the Ramsey patterns obtained with three different hairpins. With the $\frac{5}{8}$-in. hairpin, only one minimum is observed and is thus readily identified. The experimental uncertainty resulting from such a measurement then includes only one minimum of the 3-in. hairpin pattern, and that is of course the central minimum. Similarly, the central minimum of the 3-in. hairpin encom-

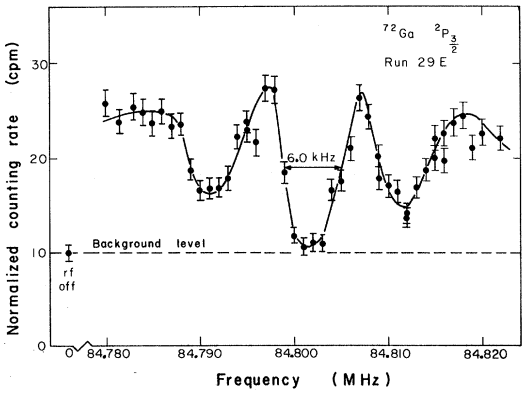

FIG. 9. A sweep of the Ramsey pattern obtained in observing the ^{72}Ga $^2P_{3/2}$ (5/2, 5/2) ⟷ (7/2, 5/2) transition with the 3-inch hairpin at 10 G.

passes only one minimum of the 6-in. hairpin pattern. Thus the procedure employed was simply to observe the central minimum with the $\frac{5}{8}$-, 3-, and 6-in. hairpins in succession. A typical result obtained with the 6-in. hairpin is shown in Fig. 10.

IV. EXPERIMENTAL RESULTS

A. Data

In each electronic state of each isotope, an attempt was made to observe at least two and sometimes three different transitions at their field-independent points. One must observe at least as many independent transitions as there are parameters to measure, and we attempted to observe one additional transition, when possible, to provide an internal check on the consistency and accuracy of our results. Each resonance was swept at least twice at a suitable rf power to establish the reproducibility of the results. The transitions observed are listed in Table I, and all the resonant frequencies observed for these transitions are listed in Table II. Also listed in Table II are the frequency of the alkali isotope which was used to calibrate the magnetic field, and the residuals ($\nu_{obs} - \nu_{calc}$) calculated with the values of the experimental parameters obtained from the final least-squares analysis.

B. Least-Squares Analysis

A least-squares fit of all the observed data to the Hamiltonian given in Eq. (1) was made (see Appendix, Subsection B). Because g_J has previously been measured by Kusch[1, 17] and because g_I, for purposes of this least-squares analysis, is best taken as the value obtained from the Fermi-Segrè relation, it was necessary to vary only the parameters a, b, and c in our analysis. For $J = \frac{1}{2}$, it was, of course, necessary only to vary a. The results of letting c vary in the $J = \frac{3}{2}$ state were inconclusive, and we may conclude that c is negligible to the accuracy of our present experiment. Thus only a and b were varied in the $J = \frac{3}{2}$ analysis.

We should also concern ourselves with any corrections to Eq. (1) required because one member of the doublet is perturbed by the other member. Fowler[18] has written a computer program to calculate these corrections, for $I = \frac{3}{2}$ and $J = \frac{3}{2}$. When applied to ^{67}Ga in the $^2P_{3/2}$ state, the calculated corrections are on the order of or smaller than the uncertainties in our results. Thus no definite conclusion can be drawn, particularly because the choice of certain parameters to be used in the calculation is somewhat arbitrary. The corrections should be even less important (compared to our experimental uncertainties) in ^{72}Ga, and the calculation was not performed for this isotope.

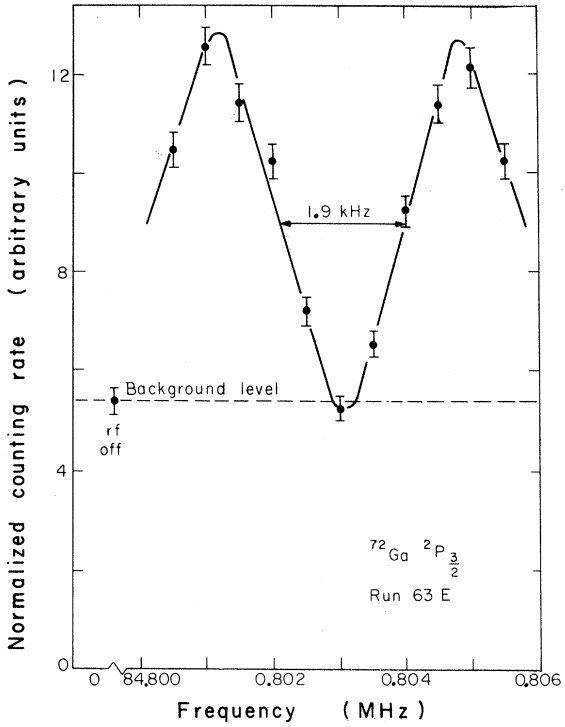

FIG. 10. A sweep of the central minimum of the Ramsey pattern corresponding to the ^{72}Ga $^2P_{3/2}$ (5/2, 5/2) ⟷ (7/2, 5/2) transition, observed with the 6-inch hairpin at 10 G. Samples with zero radio-frequency power were taken at the beginning and the end of the sweep; both were identical.

For ^{67}Ga in the $^2P_{1/2}$ state, however, it is another matter. Some of our measurements were performed at higher magnetic field (709 G) and the required field-dependent corrections are substantial. The calculation of these perturbation effects, first performed by Clendenin,[18] has been extended by Lurio to include both the oft-diagonal dipole and quadrupole matrix elements in addition to those of the magnetic field; his result is given in a paper by Eck and Kusch.[18] The largest effect of the perturbation by the $^2P_{3/2}$ level is to replace the actual value of g_I by an effective value, denoted by g_I'. Additionally, the interaction constant a obtained from a direct measurement of $\Delta\nu$, the zero-field hfs splitting, must be replaced by a corrected value, a'. Thus, for this case, a least-squares fit was made to Lurio's formula (allowing

TABLE II. Experimental data.

			Calibration data		Ga isotope data	
	Run No.	Isotope[c]	Frequency (error) (MHz)	Transition[a] label	Frequency (error) (MHz)	$\nu_{obs} - \nu_{calc}$ (kHz)
$^{67}Ga\ ^2P_{1/2}$	254*A*[b]	A	1.6000(250)	a	2457.7280(150)	−1.33
	254*B*[b]	A	3.6600(250)	a	2457.7400(400)	1.98
	257*A*[b]	A	2.1940(250)	a	2457.7400(250)	8.85
	257*B*[b]	A	2.9460(200)	a	2457.7520(200)	17.75
	60*A*	A	0.8600(150)	a	2457.7300(80)	2.14
	60*B*	A	606.5500(150)	b	2373.3213(30)	−0.17
	60*C*	A	606.5430(150)	b	2373.3215(13)	0.03
	62*E*	A	0.6270(200)	a	2457.7275(8)	−0.08
	62*F*	A	0.6140(200)	a	2457.7276(9)	0.03
$^{67}Ga\ ^2P_{3/2}$	210*A*[b]	A	1.6560(250)	d	277.8820(750)	−46.35
	210*B*[b]	A	1.6470(300)	k	278.4390(750)	44.40
	214*A*[b]	A	1.6290(250)	e	597.1700(400)	−45.07
	215*A*[b]	A	29.4260(250)	d	252.0580(400)	8.60
	220*A*[b]	A	1.8130(250)	k	278.4640(600)	36.19
	220*B*	A	1.7910(300)	d	277.8380(750)	−38.54
	248*A*[b]	A	74.9320(250)	e	575.7360(350)	−16.35
	31	B	11.0551(50)	c	263.6100(120)	1.57
	33	B	11.1178(50)	c	263.6110(70)	2.84
	40	B	11.1059(10)	c	263.6077(25)	−0.44
	43	B	11.1021(30)	c	263.6079(15)	−0.24
	44*A*	B	52.0587(60)	e	575.7530(80)	0.65
	44*B*	B	52.0555(60)	e	575.7540(60)	1.65
	55*B*	B	11.1045(70)	c	263.6077(10)	−0.44
	55*C*	B	11.1045(70)	c	263.6075(15)	−0.64
	58*A*	A	74.8820(500)	e	575.7520(25)	−0.34
	58*B*	A	74.8820(500)	e	575.7523(11)	−0.04
	62*A*	A	74.8450(200)	e	575.7523(8)	−0.06
	62*B*	A	74.8330(200)	e	575.7524(4)	0.04
	62*C*	A	29.3880(200)	d	252.0497(9)	0.34
	62*D*	A	29.3680(200)	d	252.0496(8)	0.21
$^{72}Ga\ ^2P_{1/2}$	36*A*	C	106.3590(70)	f	125.1210(30)	−3.15
	36*B*	C	106.3690(40)	f	125.1215(30)	−2.65
	36*C*	C	106.3610(150)	f	125.1210(35)	−3.15
	39*A*	B	34.9152(20)	f	125.1215(35)	−2.65
	39*B*	B	25.1970(15)	g	138.8260(30)	−0.39
	39*C*	B	25.1970(15)	g	138.8264(13)	0.01
	39*D*	B	25.1930(40)	g	138.8263(10)	−0.09
	63*F*	A	34.8410(200)	g	138.8261(9)	−0.30
	63*G*	A	34.8250(300)	g	138.8265(5)	0.09
	63*H*	A	11.1920(200)	h	152.0772(7)	0.50
$^{72}Ga\ ^2P_{3/2}$	23*A*	C	1.4031(125)	i	116.9200(150)	−1.34
	23*B*	C	1.4019(100)	i	116.9200(75)	−1.34
	23*C*	C	1.4017(100)	i	116.9210(85)	−0.34
	23*D*	C	7.3315(140)	j	84.8020(85)	−0.84
	29*A*	C	1.4059(20)	i	116.9215(25)	0.16
	29*B*	C	1.4057(20)	i	116.9215(25)	0.16
	29*C*	C	1.4047(20)	i	116.9210(20)	−0.34
	29*D*	C	1.4039(20)	i	116.9210(15)	−0.34
	29*E*	C	7.3548(30)	j	84.8015(20)	−1.41

TABLE II (*continued*)

	Calibration data			Ga isotope data		
	Run No.	Isotope	Frequency (error) (MHz)	Transition[a] label	Frequency (error) (MHz)	$\nu_{obs}-\nu_{calc}$ (kHz)
^{72}Ga $^2P_{3/2}$	29*F*	C	7.3668(60)	j	84.8018(15)	−1.18
	29*G*	C	7.3748(60)	j	84.8018(12)	−1.24
	63*A*	A	0.9040(200)	i	116.9218(15)	0.32
	63*B*	A	0.8940(200)	i	116.9217(8)	0.09
	63*C*	A	0.8850(200)	i	116.9218(7)	−0.01
	63*D*	A	4.6950(200)	j	84.8028(9)	−0.03
	63*E*	A	4.6970(200)	j	84.8031(4)	0.22

[a]Transition labels are identical to those in Table I; in addition, *k* represents (2,1) ⟷ (1,1) transitions.

[b]Old data yielding results published in Ref. 3.

[c]A = ^{85}Rb, B = ^{133}Cs, C = ^{39}K.

$\Delta\nu$ and g_I' to vary), rather than to the standard Breit-Rabi formula resulting from Eq. (1).

The result of the least-squares analysis of our data is given in Table III, where we have tabulated the values obtained for the parameters which were varied in the analysis. The constants used in the analysis are listed in Table IV.

In Table III, we have also listed the χ^2 values obtained from the least-squares fit; note that they are very low in view of the number of observations being analyzed. These low χ^2 values indicate a rather conservative assignment of uncertainties in determining the center of each resonance. However, our choice of uncertainties is based upon the confidence we have in the reproducibility and consistency of our results, taking into consideration the appearance of the resonance obtained, and the behavior of our apparatus during the experiment. In quoting our final results, we in fact increase the uncertainties obtained from our least-squares analysis by a factor of 1.5 to allow for systematic errors. We remind the reader, however, that these uncertainties are purely experimental, and do not reflect the calculational uncertainties arising from fine-structure perturbations of Eq. (1).

We thus obtain, as the final result of our experiment, the following results: for ^{67}Ga,

$$\Delta\nu(^2P_{1/2}) = 2457.727\,26(90)\ \text{MHz},$$

$$a'(^2P_{1/2}) = 1228.865\,82(45)\ \text{MHz}$$

(calculated from least-squares results for $\Delta\nu$),

$$a(^2P_{3/2}) = 175.097\,36(15)\ \text{MHz},$$

$$b(^2P_{3/2}) = 71.957\,50(55)\ \text{MHz};$$

for ^{72}Ga,

$$\Delta\nu(^2P_{1/2}) = -153.652\,66(53)\ \text{MHz},$$

$$a(^2P_{1/2}) = -43.900\,76(15)\ \text{MHz},$$

$$a(^2P_{3/2}) = -6.256\,98(11)\ \text{MHz},$$

$$b(^2P_{3/2}) = 193.673\,65(80)\ \text{MHz}.$$

C. Hyperfine-Structure Anomalies

From the results given above, we may now readily calculate the differential hfs anomalies by use of Eq. (10). We have also calculated the differential hfs anomaly for the stable isotopes of gallium, ^{69}Ga and ^{71}Ga, using the constants listed in Table IV. The results we have obtained are listed below[19]:

$$^{67}\delta^{69} = 2.51(13)\times10^{-5},$$

$$^{69}\delta^{71} = 3.15(13)\times10^{-5},$$

$$^{71}\delta^{72} = 21.2(1.8)\times10^{-5}.$$

Calculating the standard hfs anomalies for the stable gallium isotopes with the values of the interaction constants and nuclear moments listed in

TABLE III. Results of least-squares analysis.

Isotope	Electronic state	Best values of variables[a]	No. of observations	χ^2
^{67}Ga	$^2P_{1/2}$	$\Delta\nu$ = 2457.72726(60) MHz	9	1.01
		g_I' = 6.655(13)×10^{-4}		
		g_I = 6.705(13)×10^{-4}		
^{67}Ga	$^2P_{3/2}$	a = 175.09736(10) MHz	21	3.83
		b = 71.95750(36) MHz		
^{72}Ga	$^2P_{1/2}$	a = −43.90076(10) MHz	10	3.95
	$^2P_{3/2}$	a = −6.256981(69) MHz	16	2.78
		b = 193.67365(52) MHz		

[a]Uncertainties given represent one standard deviation.

TABLE IV. Values assumed for constants used in our calculations.

General	$\mu_0/h = 1.3996$ MHz/G[a]
	$M_p/M_e = 1836.1$[a]
Ga	$g_J(^2P_{1/2}) = -0.665\ 821(40)$[b]
	$g_J(^2P_{3/2}) = -1.333\ 93(11)$[b]
	$\mu_I(^{71}\text{Ga})/\mu_I(^{69}\text{Ga}) = 1.270\ 624\ 2(20)$[c]
	Diamagnetic correction $= 1.002\ 62$[d]
^{69}Ga	$I = 3/2$
	$a = 190.794\ 28(15)$ MHz[6]
	$b = 62.522\ 47(30)$ MHz[6]
	$\Delta\nu = 2677.9875(10)$ MHz[7]
	μ_0 (uncorr) $= 2.0108(3)\ \mu_N$[d]
	$Q = 0.19$ b[d]
^{71}Ga	$I = 3/2$
	$a = 242.433\ 95(20)$ MHz[6]
	$b = 39.399\ 04(40)$ MHz[6]
	$\Delta\nu = 3402.6946(13)$ MHz[7]
	μ_I (uncorr) $= 2.5549(3)\ \mu_N$[d]
	$Q = 0.12$ b[d]
^{39}K	$I = 3/2$
	$g_J = -2.002\ 295\ 4(22)$[23]
	μ_I (uncorr) $= 0.390\ 88\ \mu_N$[e]
	$\Delta\nu = 461.719\ 723(30)$ MHz[f]
^{85}Rb	$I = 5/2$
	$g_J = -2.002\ 331\ 9(20)$[23]
	μ_I (uncorr) $= 1.348\ 17\mu_N$[e]
	$\Delta\nu = 3035.732\ 439(5)$ MHz[g]
^{133}Cs	$I = 7/2$
	$g_J = -2.002\ 541\ 7(24)$[23]
	μ_I (uncorr) $= 2.5641\ \mu_N$[e]
	$\Delta\nu = 9192.631\ 770$ MHz[h]

[a] Values recommended by the NAS-NRC Committee on Fundamental Constants.

[b] Ref. 1. We have recalculated these values using the recently measured value of $g_J(^{23}\text{Na})$ (see Ref. 23).

[c] M. Rice and R. V. Pound, Phys. Rev. 99, 1036 (1955).

[d] G. H. Fuller and V. W. Cohen, Nuclear Moments (Oak Ridge National Laboratory. 1965), Appendix 1 to the Nuclear Data Sheets.

[e] I. Lindgren, Table of Nuclear Spins and Moments in Alpha-, Beta-, and Gamma-Ray Spectroscopy, edited by K. Siegbahn (North-Holland Publishing Co., Amsterdam, 1965), Vol. 2, p. 1621.

[f] S. Penselin, private communication.

[g] S. Penselin, T. Moran, V. W. Cohen, and G. Winkley, Phys. Rev. 127, 524 (1962).

[h] The ^{133}Cs $\Delta\nu$ is the presently accepted frequency standard.

Table IV, we obtain the following results[19]:

$$^{69}\Delta^{71}(^2P_{1/2}) = 6.2(1.7)\times10^{-6},$$

$$^{69}\Delta^{71}(^2P_{3/2}) = 2.52(19)\times10^{-5}.$$

As mentioned above, we can now use these to determine the ratio of these same quantities in our radioactive gallium isotopes, and thus determine the actual values of our radioactive hfs anomalies. However, rather than simply taking the ratio of these anomalies for the stable isotopes, we may make a more accurate determination by using the ratio of the anomaly in the $^2P_{3/2}$ state to the differential hfs anomaly, as the relative uncertainties of these quantities are smaller. Doing this, we obtain

$$^{69}\Delta^{71}(^2P_{3/2})/^{69}\delta^{71} = 0.80(7). \quad (11)$$

This may be compared with the theoretical value[5] of -0.76. The close agreement of these values gives us confidence in the methods developed by Schwartz[5] and used in our analysis.

Assuming now that this ratio is constant for all isotopes in gallium, we obtain

$$^{67}\Delta^{69}(^2P_{3/2}) = 2.01(20)\times10^{-5},$$
$$\text{and } ^{71}\Delta^{72}(^2P_{3/2}) = 17.0(2.0)\times10^{-5}. \quad (12)$$

For the $^2P_{1/2}$ state, we note that experimentally

$$^{69}\Delta^{71}(^2P_{1/2})/^{69}\delta^{71} = 0.20(6). \quad (13)$$

Once again, assuming this ratio constant for all the isotopes of gallium, we obtain from our observed differential hfs anomaly for the $^2P_{1/2}$ state the values

$$^{67}\Delta^{69}(^2P_{1/2}) = 0.50(14)\times10^{-5}$$
$$^{71}\Delta^{72}(^2P_{1/2}) = 4.2(1.2)\times10^{-5}. \quad (14)$$

D. Nuclear Moments

The foregoing calculation of the hfs anomalies now allows us to calculate the nuclear magnetic dipole moments of ^{67}Ga and ^{72}Ga very accurately, as it allows us to correct for the deviations from the Fermi-Segrè formula used to calculate the values of these moments from our measured hfs interaction constants. In effect, then, we are using Eq. (7) above to calculate the nuclear g factor, and hence the nuclear magnetic moment, from our measured value of a and our calculated value of Δ, also making use of a and g_I for the stable isotopes. Applying this method, we obtain, for ^{67}Ga,

$$\mu_I(\text{uncorr}) = 1.8454(3)\mu_N,$$

and, for ^{72}Ga,

$$\mu_I(\text{uncorr}) = -0.131\ 86(2)\mu_N.$$

These values are now corrected for the effect of the hfs anomaly, but the diamagnetic correction has not been included. If we include the diamagnetic correction given in Table IV, we obtain for ^{67}Ga

$$\mu_I(\text{corr}) = 1.8502(4)\mu_N,$$

and for ^{72}Ga

$$\mu_I(\text{corr}) = 0.132\ 20(3)\mu_N,$$

where we have assumed a 5% uncertainty in the value of the added diamagnetic correction.

The uncertainties assigned to these values of the moments result only from the uncertainties in the measured values of the nuclear moments for the stable isotopes (see Table IV). Should these values later be measured to higher precision, one can then immediately use our hfs separations to recal-

culate the nuclear moments of ^{67}Ga and ^{72}Ga to higher precision.

Applying Eq. (6) to our results for the electric quadrupole interaction constant, we obtain

$$Q(^{69}\mathrm{Ga}) = +0.22 \text{ b}$$

and $Q(^{72}\mathrm{Ga}) = +0.59$ b.

No uncertainty is included with this result, as the uncertainty resides entirely in the calculation of the quadrupole moment for the stable isotopes[9] and no estimate has been made of this uncertainty.

V. CONCLUSIONS

A. Nuclear Moments

The nuclear spin of ^{67}Ga has long been explained as due to an odd $2p_{3/2}$ proton. Configuration-mixing calculation of the nuclear moments and comparison with experimental results favors assignment of the $(1f_{7/2})^8\ (2p_{3/2})^3$ configuration for ^{67}Ga and ^{69}Ga, while the $(1f_{7/2})^8\ (1f_{3/2})^2\ 2p_{3/2}$ configuration is favored[13] for ^{71}Ga. More recent calculations,[20] including the effects of the pairing interaction, yield values consistent with the experimental magnetic dipole moments of both ^{67}Ga and ^{69}Ga.

The case of ^{72}Ga is much more puzzling, and in fact the measured nuclear moment of ^{72}Ga has long caused difficulty for nuclear theory. At present, this difficulty has not been resolved, and no reasonable configuration results in a calculated value of the nuclear magnetic moment in agreement with the experimental value.[21]

The calculated value for the quadrupole moment of ^{67}Ga is in reasonable agreement with the experimental results. For ^{72}Ga, B. J. Raz[22] has calculated a quadrupole moment of 0.58 b, in close agreement with our experimental value of 0.59 b.

B. Hyperfine-Structure Anomalies

Because of the extremely small size of the hfs anomalies for atoms in P states, the theoretical interpretation is less clear than in the case of the nuclear moments. Stroke *et al.*[13] have calculated the Bohr-Weisskopf anomalies expected for the two configurations mentioned above, and have obtained $\Delta(^2P_{1/2}) = 0 \pm 5 \times 10^{-6}$ for the first configuration, and $\Delta(^2P_{1/2}) = (-1 \pm 1) \times 10^{-5}$ for the second configuration. One would expect a Breit-Rosenthal anomaly of roughly the same size. Since the uncertainties for their calculations are approximately the same as our experimental results for the anomalies, little can be deduced from this result. However, from the values Stroke *et al.* calculate for the b coefficient and the $\mathcal{I}_n'$ radial integrals, we would expect that $^{67}\Delta^{69}$ would be approximately equal to $^{69}\Delta^{71}$. This is in agreement with our experimental observation. The situation for ^{72}Ga is more complex, due to the odd-odd nature of this isotope. It is interesting to note that the anomaly is a factor of 10 larger than the others quoted above, while the nuclear moment is a factor 10 smaller. This is not too surprising, as one would expect a considerable difference in the distribution of nuclear magnetism and charge for ^{72}Ga as compared with ^{71}Ga, in view of the observed small magnetic dipole moment and large quadrupole moment.

ACKNOWLEDGMENTS

We gratefully acknowledge the assistance of Dana Vance in his careful and competent counting of the radioactive samples and plotting of the data. We also appreciate the assistance given by Mrs. Patricia Shaw in supervising the safe handling of these radioisotopes, and by Tom Geballe in improving the computer programs. We thank Mrs. Julia Taylor for her excellent typing of the manuscript. One of us (VJE) particularly wishes to express his appreciation to Professor William A. Nierenberg for several stimulating discussions during the very early portions of this experiment, and for his constant encouragement.

APPENDIX

A. Hairpin Characterisitcs

In performing experiments of high precision, it is essential that all systematic errors be detected and eliminated. A major source of systematic error in atomic-beam research arises from distortion and shifting of resonance lines, usually caused by either (a) poor hairpin design, or (b) application of too much radio-frequency power. The hairpins used in this experiment were of a new design, and therefore we tested them thoroughly before use. Because we believe the test results will be of interest to other workers in this field, and because they graphically illustrate the importance of using the proper amount of radio-frequency power to excite the transition, we include here a brief summary of the results.

The hairpins used in this experiment were of two types: a $\frac{5}{8}$-in. rigid coaxial air line,[23] and a 3-in. and a 6-in. hairpin of the type shown in Fig. 2. Because the shorter hairpins were used only for preliminary measurements, the long 6-in. hairpin was tested most carefully. The method used was to look at field-independent transitions in ^{39}K; in this isotope the $\Delta F = 1$ transition frequencies are conveniently low ($\approx$450 MHz), but yet are higher than most of the frequencies required in the gallium observations. Both $\Delta m = \pm 1$ and $\Delta m = 0$ resonances were traced out at various radio-frequency powers. The results are shown in Figs. 11 and 12. A plot of resonance height versus rf power is shown in Fig. 4 for a $\Delta m = 1$ transition, and in Fig. 13 for a $\Delta m = 0$ transition. It is apparent that great care must be exercised to avoid over-powering observed resonances. Although excess-power effects are immediately apparent when working with stable atoms, they are not easily detected with radioactive isotopes. Thus it is essential to measure the optimum power for each radioisotope resonance by tracing out a curve such as Fig. 6.

Although the center minimum of the $\Delta m = 0$ resonance did not shift as rf power was increased, the side minima and maxima did shift outward from the center.

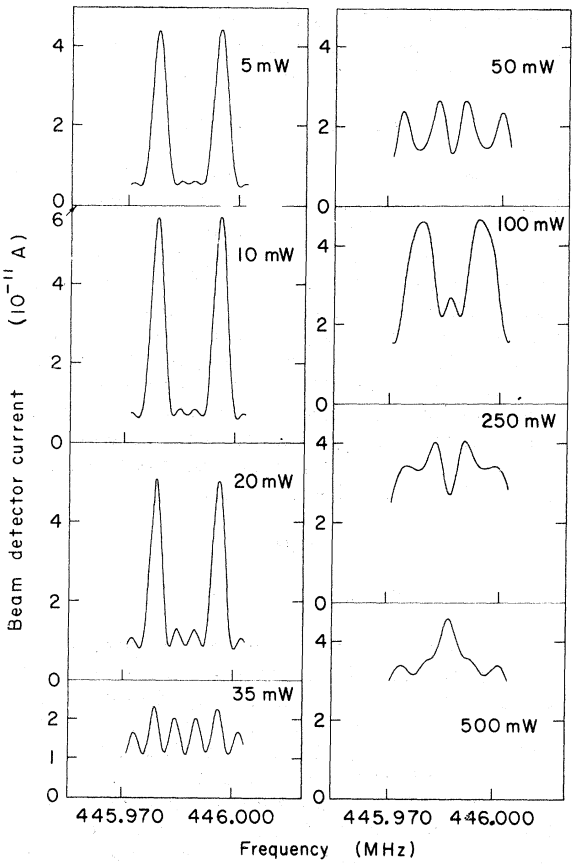

FIG. 11. Observation of the ^{39}K doublet (2, −1) ⟷ (1, 0), (2, 0) ⟷ (1, −1) as a function of rf power. Hairpin length: 6 inch. As rf power is increased, the two resonances broaden and become distorted until they merge and become indistinguishable.

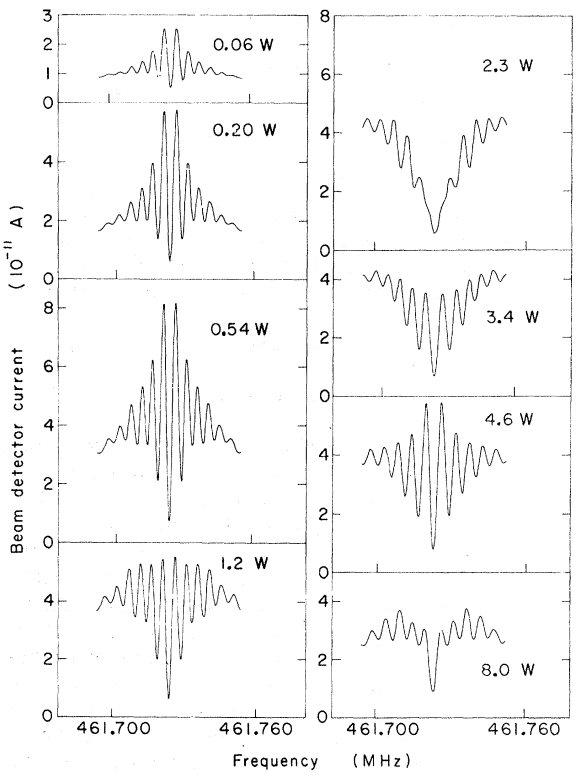

FIG. 12. Observation of the ^{39}K (2,0) ⟷ (1,0) transition as rf power is increased. Hairpin length: 6 inches.

The high-frequency behavior of the hairpins was tested by observing the $\Delta F = \pm 1$ transitions of ^{85}Rb. The observed $\Delta m = \pm 1$ resonances (≈ 2600 MHz) are shown in Fig. 14 for the three different hairpins, and the $\Delta m = 0$ resonances (≈ 3000 MHz) are shown in Fig. 15. It is clear that the 6-in. hairpin is unsatisfactory at these frequencies, but the 3-in. device appears to be acceptable. The wavelength is about 4 in. at these frequencies, and most likely standing-wave patterns are set up in the 6-in. hairpin, leading to the anomalous line shapes.

B. Computational Methods

Because our computer routines have been considerably modified since they were last described in the literature,[24] and because they are now in use in a number of laboratories throughout the world, we believe it desirable to summarize the main features of our present computational methods.

Three basic computational problems are encountered in atomic-beam research: (a) calculating the frequency of transition between two energy levels of the Hamiltonian given in Eq. (1), (b) calculating the probability for such a transition to occur, and (c) performing a least-squares fit of the adjustable parameters to the observed data.

Transition Frequencies

To calculate transition frequencies, we must obtain the eigenvalues of Eq. (1). A method has been developed which takes advantage of two particular properties of the matrix representing this Hamiltonian: (a) it may be arranged in block form, with each submatrix corresponding to a given m value, and (b) within each submatrix, all elements that are more than 1 off the diagonal are zero.

Upon examining Eq. (1), we see that the diagonal matrix elements of the Hamiltonian are

$$A_p = \langle Fm | \mathcal{H} | Fm \rangle = aa_p + bb_p + cc_p + (-g_J + g_I)(\mu_0/h)Hd_p - g_I(\mu_0/h)Hm, \tag{A1}$$

where

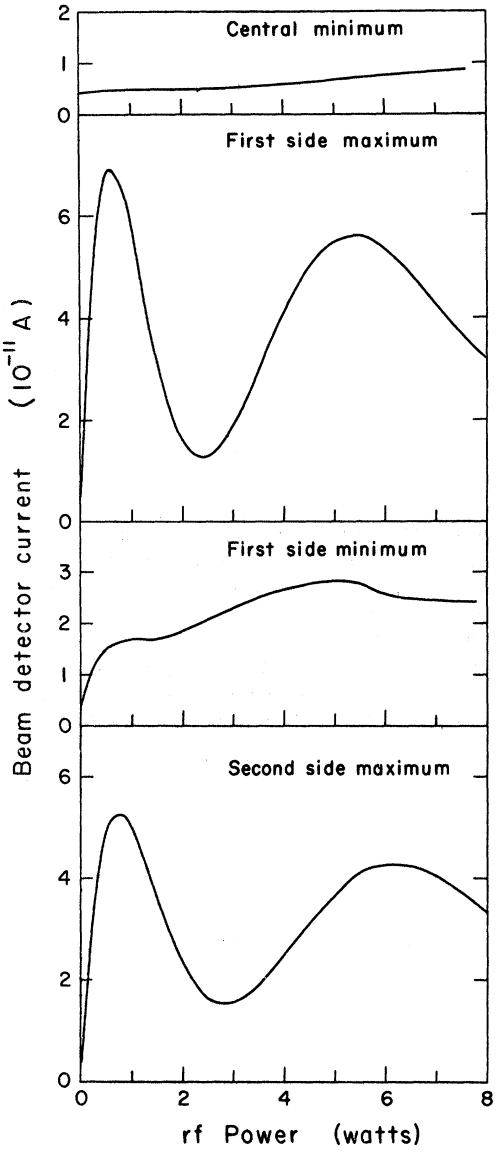

FIG. 13. Height of various points on the Ramsey-pattern resonance shown in Fig. 12, as a function of rf power. The signal level at zero rf power indicates the detector background. A similar curve obtained for a $\Delta m = \pm 1$ transition in ^{39}K is shown in Fig. 4.

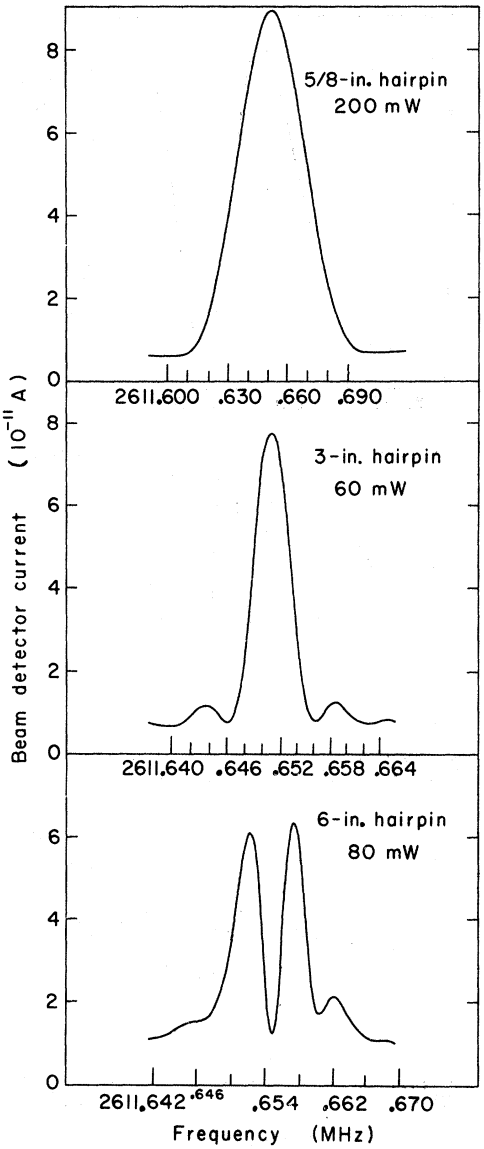

FIG. 14. The ^{85}Rb (3,1) ⟷ (2,-2) resonances obtained with various hairpins. The severe distortion of the resonance obtained with the 6-inch hairpin is evident. The frequency displacements from one trace to another result from changes of the magnetic field between the successive days on which the traces were obtained. All sweeps were made at optimum rf power.

$$a_p = \langle Fm | \vec{I}\cdot\vec{J} | Fm \rangle = \tfrac{1}{2}[F(F+1) - I(I+1) - J(J+1)], \tag{A2}$$

$$b_p = \langle Fm | Q_{\mathrm{op}} | Fm \rangle = [3a_p^{\,2} + \tfrac{3}{2}a_p - I(I+1)J(J+1)][2I(2I-1)J(2J-1)]^{-1}, \tag{A3}$$

$$c_p = \langle Fm | \mathcal{O}_{\mathrm{op}} | Fm \rangle = \{10a_p^{\,3} + 20a_p^{\,2} + 2a_p[-3I(I+1)J(J+1) + I(I+1) + J(J+1) + 3] - 4I(I+1)J(J+1)\}$$
$$\times [I(I-1)(2I-1)J(J-1)(2J-1)]^{-1} \tag{A4}$$

$$d_p = \langle Fm | J_z | Fm \rangle = m[F(F+1) + J(J+1) - I(I+1)]/2F(F+1) \tag{A5}$$

and $p = 1$ for $F = F_{\min}$, $p = 2$ for $F = F_{\min} + 1$, etc. The square of the matrix elements 1 off the diagonal is given by

$$e_p = \langle Fm | \mathcal{H} | F+1, m \rangle^2$$

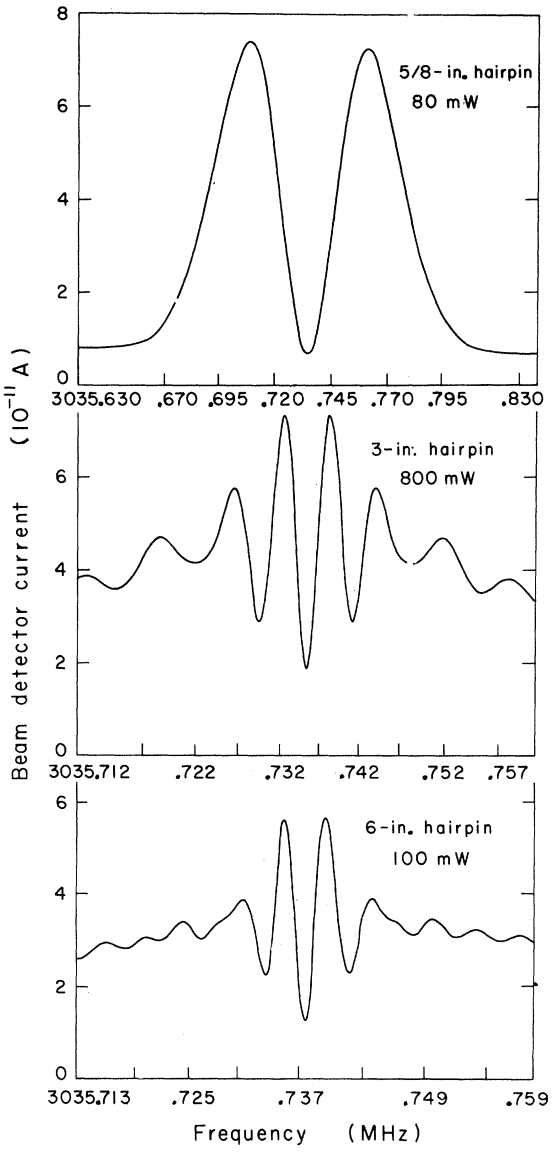

FIG. 15. The ^{85}Rb (3,0) ⟷ (2,0) resonances obtained with various hairpins. Note the distortion of the second side maxima when using the 6-inch hairpin. The displacements in frequency from one trace to another result from changes of the magnetic field between the successive days on which the traces were obtained. All curves were taken at optimum rf power. Similar resonances obtained for ^{39}K are shown in Fig. 3.

$$= [(-g_J + g_I)(\mu_0/h)H]^2 (F+1-I+J)(F+1-I+J)(I+J+2+F)$$

$$\times (I+J-F)(F+1-m)(F+1+m)[4(F+1)^2(2F+3)(2F+1)]^{-1}. \quad \text{(A6)}$$

We require the solution of the N-dimensional secular determinant

$$D_N = |H_N - IE(F,m)| = 0, \quad \text{(A7)}$$

where H_N is the particular N-dimensional submatrix under consideration, $E(F,m)$ is the eigenvalue of that submatrix corresponding to the quantum numbers (F,m), and I is the identity matrix. The method of solution is given in Ref. 24. It involves the use of the recursion relations

$$D_p = (A_p - E)D_{p-1} - e_{p-1}D_{p-2}, \quad \text{(A8)}$$

where by definition $D_0 = 1$ and $D_{-1} = 0$, and

$$\partial D_p/\partial E = (A_p - E)(\partial D_{p-1}/\partial E) - e_{p-1}(\partial D_{p-2}/\partial E) - D_{p-1}. \quad \text{(A9)}$$

For a particular trial value of E, D_N and $\partial D_N/\partial E$ can be calculated by repeated application of Eqs. (A8) and (A9). An improved value of E can then be obtained by Newton's method

$$E_{i+1} = E_i - D_N/(\partial D_N/\partial E). \quad \text{(A10)}$$

Repetition of this process then yields improved values for $E(F, m)$ which approach any desired precision.

The initial trial value of E is selected by beginning the computation at zero magnetic field, where $e_p = 0$ and the roots are easily identified [$E(F, m) = A_p(F, m)$ for $H = 0$]. The eigenvalues E are then calculated at increasing values of H until the desired magnetic field is obtained. Finally the desired frequency is given by

$$\nu(F, m \rightarrow F', m') = E(F, m) - E(F', m'). \tag{A11}$$

In addition, the standard program calculates other derivatives of interest, namely $\partial\nu/\partial H$, $\partial\nu/\partial a$, $\partial\nu/\partial b$, $\partial\nu/\partial c$, $\partial\nu/\partial g_I$, and $\partial\nu/\partial g_J$. The procedure used to compute these derivatives is to obtain various recursion relations involving derivatives of D_N, and then to use these to compute the desired derivatives. For example, we obtain $\partial\nu/\partial a$ from

$$\partial\nu/\partial a = \partial E(F, m)/\partial a - \partial E(F', m')/\partial a\ , \tag{A12}$$

$$\partial E/\partial a = -(\partial D_N/\partial a)/(\partial D_N/\partial E)\ , \tag{A13}$$

$$\partial D_p/\partial a = (A_p - E)(\partial D_{p-1}/\partial a) + a_p D_{p-1} - e_{p-1}(\partial D_{p-2}/\partial a)\ , \tag{A14}$$

and by using $\partial D_p/\partial E$ from Eq. (A9).

Transition Probabilities

The probability of inducing an hfs magnetic-dipole transition from state a_i to state a_j by use of an oscillating rf field $H_1 = H_0 \exp i\omega t$ is proportional to $g_J{}^2 H_0{}^2 \langle a_i | \vec{J} | a_j \rangle^2$, for rf powers such that the transition is well below saturation (neglecting the effect of the nuclear moment).[15] Thus by calculating $\langle a_i | \vec{J} | a_j \rangle$ we obtain a convenient parameter indicating the relative magnitude of the transition probability. For $\Delta m = 0$ transitions, we need only $\langle a_i | J_z | a_j \rangle$; for $\Delta m = \pm 1$ we require $\langle a_i | J_x | a_j \rangle$.

For $H > 0$, we can express $\langle a_i | \vec{J} | a_j \rangle$ in terms of the matrix elements of $\vec{J}$ between states at $H = 0$, i.e., in terms of the elements $\langle F_k m_k | \vec{J} | F_l m_l \rangle$ of the (F, m) representation. We have

$$\langle a_i | \vec{J} | a_j \rangle = \sum_{k,l} \langle a_i | F_k m_k \rangle \langle F_k m_k | \vec{J} | F_l m_l \rangle \langle F_l m_l | a_j \rangle\ . \tag{A15}$$

Because the elements $\langle F_k m_k | \vec{J} | F_l m_l \rangle$ at $H = 0$ are well known,[14] our problem thus reduces to determining the coefficients $\langle a_i | F_k m_k \rangle$. But these are the components of the eigenvector $|a_i\rangle$ satisfying the equation $\mathcal{H}|a_i\rangle = E_i |a_i\rangle$, or $(\mathcal{H} - E_i)|a_i\rangle = 0$. Writing this out in terms of the matrix elements listed in Eqs. (A1)–(A6), we have

$$\begin{bmatrix}
A_N - E_i & (e_{N-1})^{1/2} & 0 & 0 & \cdot & \cdot & \cdot \\
(e_{N-1})^{1/2} & A_{N-1} - E_i & (e_{N-2})^{1/2} & 0 & \cdot & \cdot & \cdot \\
0 & (e_{N-2})^{1/2} & A_{N-2} - E_i & (e_{N-3})^{1/2} & \cdot & \cdot & \cdot \\
0 & 0 & (e_{N-3})^{1/2} & A_{N-3} - E_i & & & \\
 & & & & \ddots & & \\
\cdot & \cdot & & & A_3 - E_i & (e_2)^{1/2} & 0 \\
\cdot & \cdot & & & (e_2)^{1/2} & A_2 - E_i & (e_1)^{1/2} \\
\cdot & \cdot & & & 0 & (e_1)^{1/2} & A_1 - E_i
\end{bmatrix}
\begin{bmatrix}
\langle a_i | F_N m \rangle \\
\langle a_i | F_{N-1} m \rangle \\
 \\
 \\
 \\
\langle a_i | F_3 m \rangle \\
\langle a_i | F_2 m \rangle \\
\langle a_i | F_1 m \rangle
\end{bmatrix} = 0. \tag{A16}$$

Nierenberg[25] has deduced that an unnormalized solution to this equation is

$$\langle a_i | F_N m \rangle = D_{N-1},\ \langle a_i | F_{N-1} m \rangle = -(e_{N-1})^{1/2} D_{N-2},\ \langle a_i | F_{N-2} m \rangle = (e_{N-1} e_{N-2})^{1/2} D_{N-3}, \cdots$$

$$\langle a_i | F_2 m \rangle = (-1)^N (e_{N-1} e_{N-2} \cdots e_2)^{1/2} D_1,\ \langle a_i | F_1 m \rangle = (-1)^{N+1} (e_{N-1} e_{N-2} \cdots e_2 e_1)^{1/2},$$

where D_P is the determinant given by Eqs. (A7) and (A8). Thus we see that the particularly simple form of our Hamiltonian matrix allows us to calculate the $\langle a_i | F_k m_k \rangle$ and thus the $\langle a_i | \vec{J} | a_j \rangle$ in terms of quantities previously obtained when computing transition frequencies.

Least-Squares Analysis

The information gained from a typical atomic-beam experiment consists of many sets of data, with each set made up of (a) a measurement of a magnetic field (measured in terms of the resonant frequency of a known transition in a calibration material) and (b) a measurement of the resonant frequency of a particular transition in the isotope under study. This latter frequency depends upon the values of the parameters a, b, c, g_I, and g_J for that isotope, and thus a measurement of this frequency provides information about the actual values of these parameters. Because there are many such sets of data, involving observation of various transitions at several magnetic fields, and because each of these transitions has a different dependence upon the parameters of the Hamiltonian, it is desirable to develop a method of simultaneously fitting all the data to the Hamiltonian, Eq. (1). The least-squares method offers such a standard objective procedure.

The principle of least squares requires that the quantity

$$Q=\sum_i[\nu_i - f_i(a,\ b,\ c, g_I g_J)]^2\omega_i \tag{A18}$$

be a minimum for the best-fit values a, b, c, g_I, and g_J. Here the sum runs over all sets of data i, ν_i is the experimentally observed resonant frequency for a transition, f_i is the value calculated [from Eq. (1)] for that frequency for the given values of a, b, c, g_I, and g_J, and ω_i is the measure of precision of the observation (the so-called statistical weight). One long-standing definition of the measure of precision of a single observation is $\omega_i = 1/\sigma_i^2$, where σ_i^2 is the variance (σ_i = standard deviation), and indicates that the observation comes from a population whose distribution is given by

$$P(\nu) = (2\pi\sigma^2)^{-1/2} \exp[-(\nu-\xi)^2/2\sigma^2], \tag{A19}$$

where ξ is the mean value of ν.

Because the parent population must normally be inferred from a single sweep of a resonance, the measure of precision of the peak position is compounded from a fixed fraction ($\Delta\nu_i$) of the resonance linewidth and from a quantity (ΔH) describing the uncertainty in the magnetic field,

$$\omega_i = (\sigma_{\nu_i}{}^2 + \sigma_{H_i}{}^2)^{-1} = [(\Delta\nu_i)^2 + (\partial f_i/\partial H)^2(\Delta H_i)^2]^{-1}. \tag{A20}$$

The technique used to minimize the function Q follows a method outlined by Nierenberg.[26] If we have a function Q of n variables $x_1, \cdots, x_n$, the condition for a minimum of $Q(x_1, \cdots, x_n)$ is that $dQ=0$, or $\partial Q/\partial x_i = 0$ for all i (assuming the x_i to be independent). Expanding the $\partial Q/\partial x_i$ about their minimum at $x_1{}^0, \ldots, x_n{}^0$, we see

$$\frac{\partial Q}{\partial x_i} = \frac{\partial Q}{\partial x_i}\bigg|_{x_i{}^0} + \sum_{j=1}^{n}(x_j - x_j{}^0)\frac{\partial^2 Q}{\partial x_i \partial x_j}\bigg|_{x_i{}^0, x_j{}^0} + \cdots. \tag{A21}$$

By definition $\left.\dfrac{\partial Q}{\partial x_i}\right|_{x_i{}^0} = 0.$

Letting $\delta x_j = x_j - x_j{}^0$, denoting $\left.\dfrac{\partial^2 Q}{\partial x_i \partial x_j}\right|_{x_i{}^0, x_j{}^0}$ by $\dfrac{\partial^2 Q_0}{\partial x_i x_j}$, and ignoring higher-order terms, we see that

$$\frac{\partial Q}{\partial x_i} = \sum_{j=1}^{n} \delta x_j \frac{\partial^2 Q_0}{\partial x_i \partial x_j}. \tag{A22}$$

For $i=1, \cdots, n$, we get a set of n equations in the n unknowns δx_i. If we let $\underline{R}$ be the $(n\times n)$ matrix with elements $R_{ij} = \frac{1}{2}(\partial^2 Q_0/\partial x_i \partial x_j)$, let $\underline{\delta}$ be the column matrix with elements δx_i, and $\underline{P}$ the column matrix with elements $\frac{1}{2}(\partial Q/\partial x_i)$, then we see that $\underline{P} = \underline{R}\ \underline{\delta}$, and the solution for $\underline{\delta}$ is

$$\underline{\delta} = \underline{R}^{-1}\underline{P}. \tag{A23}$$

Note that the relation $P = R\delta$ differs from the set of Eqs. (A22) by inclusion of a factor $\frac{1}{2}$ on both sides of the equation. Although this alters neither the equation nor the values of the δx_i obtained as solutions, this factor must be inserted at this point if we are to interpret R^{-1} as the variance-covariance matrix, where the variances and covariances have the customary meanings assigned them in the standard linear (Gauss) least-squares procedure.

Thus by selecting trial values for the x_i, evaluating $\underline{R}$ and $\underline{P}$ for these x_i, and solving for the δx_i, we obtain new trial values given by

$$x_i' = x_i - \delta x_i . \tag{A24}$$

This process is repeated until the δx_i become arbitrarily small; the resulting values of the x_i then yield the minimum value for Q.

This minimization method proceeds in a quadratic fashion as contrasted to the standard linear (Gauss) method. Thus it approaches the minimum more rapidly, but involves the added complexity of calculating the second derivatives. For the problem at hand, the advantages of the quadratic method outweigh the disadvantages.

The variance-covariance matrix is given by R^{-1}. The diagonal elements are the variances of the fitted variables [i.e., $(R^{-1})_{ii} = \sigma_{x_i}^2$] and the off-diagonal elements are the covariances [i.e., $(R^{-1})_{ij} = \rho_{ij}\sigma_{x_i}\sigma_{x_j}$, where the ρ_{ij} are the coefficients of correlation]. These quantities may be determined from the matrix R by

$$(R^{-1})_{ij} = (\text{cofactor } R_{ji})/|R| . \tag{A25}$$

The value of Q at its minimum is denoted by χ^2. The χ^2 is important in the analysis, because its distribution function can be calculated. From its distribution function its average value is the number of degrees of freedom $= k - n$, where k = number of observations and n = number of variables. The variance on χ^2 is $2(k-n)$. A consistency factor $[\chi^2/(k-n)]^{1/2}$ is expected to be $1 \pm [1/2(k-n)]^{1/2}$. There is a probability of 68% that the value of the consistency factor will lie within the error interval. If the consistency factor of a fit is much smaller than unity, it is probable that the σ_i attached to the input data are very conservative. On the other hand, if the consistency factor is improbably large, the input data may be less reliable than supposed, or certain data may be inconsistent. It is also possible that a large χ^2 may result from attempting to fit an incorrect functional form to the data. After inconsistent data are ruled out, the proper procedure is to multiply the variance-covariance matrix by the value of $\chi^2/(k-n)$. The result is called the error matrix by external consistency. [We generally ignore the factor $\chi^2/(k-n)$ if it is less than 1 and include it if it is greater than 1.] The square roots of the diagonal elements of the error matrix are then the standard deviations of the fitted parameters.

The residuals of the fit are the $\nu_i - f_i(x_i, \cdots, x_n)$ calculated for the best-fit values of the x_i. A careful examination of the residuals will frequently result in detection of inconsistent data (usually resulting from incorrect preliminary calculations), and also often aids in the discovery of systematic errors.

The foregoing discussion has been general, involving n parameters $x_i, \cdots, x_n$. For the specific problem of fitting our data to Eq. (1), the x_i are a, b, c, g_I, and g_J. The derivatives required in the solution of Eq. (A23) are obtained from Eq. (A8) in a manner analogous to that used to derive Eqs. (A9) and (A14).

To illustrate the foregoing discussion, consider the simple case when c, g_I, and g_J are known and may be held fixed, while a and b are the parameters to be varied in the minimization procedure. The $\partial Q/\partial a$ may be calculated by use of Eq. (A12), and the other required derivatives (e.g., $\partial^2 Q/\partial a^2$, $\partial^2 Q/\partial a \partial b$, etc.) may be similarly computed. The Eqs. (A22) become

$$\frac{\partial Q}{\partial a} = \frac{\partial^2 Q}{\partial a^2}\delta a + \frac{\partial^2 Q}{\partial a \partial b}\delta b, \quad \frac{\partial Q}{\partial b} = \frac{\partial^2 Q}{\partial b \partial a}\delta a + \frac{\partial^2 Q}{\partial b^2}\delta b, \tag{A26}$$

and the matrices $\underline{R}$, $\underline{\delta}$, and $\underline{P}$ are given by

$$\underline{R} = \begin{pmatrix} \frac{1}{2}\partial^2 Q/\partial a^2 & \frac{1}{2}\partial^2 Q/\partial a \partial b \\ \frac{1}{2}\partial^2 Q/\partial b \partial a & \frac{1}{2}\partial^2 Q/\partial b^2 \end{pmatrix}, \quad \underline{\delta} = \begin{pmatrix} \delta a \\ \delta b \end{pmatrix}, \quad \text{and } \underline{P} = \begin{pmatrix} \frac{1}{2}\partial Q/\partial a \\ \frac{1}{2}\partial Q/\partial b \end{pmatrix}, \tag{A27}$$

The variance-covariance matrix has the form

$$R^{-1} = \begin{pmatrix} \sigma_a^2 & \rho\sigma_a\sigma_b \\ \rho\sigma_a\sigma_b & \sigma_b^2 \end{pmatrix}, \tag{A28}$$

where the elements are obtained by use of Eq. (A25). For example, the variances are given by

$$\sigma_a^2 = (R^{-1})_{11} = (\text{cofactor} R_{11})/|R| = \tfrac{1}{2}(\partial^2 Q/\partial b^2)/|R|$$

$$\text{and} \quad \sigma_b^2 = (R^{-1})_{22} = (\text{cofactor} R_{22})/|R| = \tfrac{1}{2}(\partial^2 Q/\partial a^2)/|R| . \tag{A29}$$

In summary, the least-squares analysis is performed by minimizing the function Q given in Eq. (A18), using a quadratic method of generating new trial values from given trial values of the pertinent parameters. The method of calculating all the required derivatives and eigenvalues is based upon the recursion formula, Eq. (A8), with Newton's method used to calculate the energy eigenvalues. The net result of the procedure is to produce the values of the parameters that yield a minimum value for Q, which is then the χ^2 of the fit. The standard deviations σ_i are then obtained from the variances that are diagonal elements of the variance-covariance matrix.

*Research supported by the U. S. Atomic Energy Commission.

†Present address: Department of Physics, Calvin College, Grand Rapids, Michigan.

‡Present address: Department of Physics, Middle East Technical University, Ankara, Turkey.

[1]P. Kusch and H. M. Foley, Phys. Rev. 74, 250 (1948).

[2]A. Lurio and A. G. Prodell, Bull. Am. Phys. Soc. 30, 13 (1955).

[3]V. J. Ehlers and W. A. Nierenberg, Bull. Am. Phys. Soc. 4, 452 (1959); Bull. Am. Phys. Soc. 5, 214 (E) (1960)

[4]V. J. Ehlers, H. A. Shugart, and O. Tezer, Bull. Am. Phys. Soc. 12, 905 (1967); V. J. Ehlers, Y. Kabasakal, and H. A. Shugart, Bull. Am. Phys. Soc. 12, 925 (1967).

[5]C. Schwartz, Phys. Rev. 99, 1035 (1955).

[6]R. T. Daly, Jr., and J. H. Holloway, Phys. Rev. 96, 539 (1954).

[7]A. Lurio and A. G. Prodell, Phys. Rev. 101, 79 (1956).

[8]G. Breit and I. I. Rabi, Phys. Rev. 38, 2082 (1931).

[9]G. F. Koster, Phys. Rev. 86, 148 (1952).

[10]H. B. G. Casimir, On the Interaction Between Atomic Nuclei and Electrons (W. H. Freeman & Co., San Francisco, 1963).

[11]A. Bohr and V. F. Weisskopf, Phys. Rev. 77, 94 (1950).

[12]G. Breit and J. E. Rosenthal, Phys. Rev. 41, 459 (1932).

[13]H. H. Stroke, R. J. Blin-Stoyle, and V. Jaccarino, Phys. Rev. 123, 1326 (1961); J. Eisinger and V. Jaccarino, Rev. Mod. Phys. 30, 528 (1958).

[14]N. F. Ramsey, Molecular Beams (Oxford University Press, London, 1956).

[15]W. J. Childs, L. S. Goodman, and L. J. Kieffer, Phys. Rev. 120, 2138 (1960).

[16]J. L. Worcester, J. C. Hubbs, and W. A. Nierenberg, Bull. Am. Phys. Soc. 2, 316 (1957).

[17]We are presently remeasuring g_J for the stable gallium isotopes. Preliminary values are in good agreement with Kusch's values.

[18]Fowler, Thomas R., Lawrence Radiation Laboratory Report No. UCRL-18331, 1968 (unpublished); W. W. Clendenin, Phys. Rev. 94, 1590 (1954); T. G. Eck and P. Kusch, Phys. Rev. 106, 958 (1957).

[19]The uncertainties we have given for ${}^{69}\delta^{71}$, ${}^{69}\Delta^{71}({}^2P_{1/2})$, and ${}^{69}\Delta^{71}({}^2P_{3/2})$ are different from those given in Refs. 4, 5, and 7. We have obtained these uncertainties by taking the square root of the sum of the squares of the relative uncertainties quoted for the parameters entering into the calculation of these quantities, whereas the other authors apparently summed the relative uncertainties.

[20]N. Freed and L. S. Kisslinger, Nucl. Phys. 25, 611 (1961).

[21]A. A. Ross-Bonney, private communication.

[22]B. J. Raz, private communication quoted in Ref. 15.

[23]P. A. Vanden Bout, E. Aygun, V. J. Ehlers, T. Incesu, A. Saplakoglu, and H. A. Shugart, Phys. Rev. 165, 88 (1968).

[24]H. L. Garvin, T. M. Green, E. Lipworth, and W. A. Nierenberg, Phys. Rev. 116, 393 (1959).

[25]W. A. Nierenberg (University of California-San Diego), private communication.

[26]W. A. Nierenberg, Lawrence Radiation Laboratory Report No. UCRL-3816 (revised), 1959 (unpublished).

PHYSICAL REVIEW VOLUME 176, NUMBER 1 5 DECEMBER 1968

Effect of an External Radiation on the Energy Levels of an Electron System*

B. L. Jones and M. Verschueren

Department of Physics, Simon Fraser University, Burnaby, British Columbia, Canada

(Received 8 July 1968)

The effect of an external radiation on the energy levels of an electron system is treated by a Green's-function technique. The external radiation is treated classically and is assumed to be totally incoherent. Using the statistical properties of the external radiation, an averaged one-electron Green's function which describes the properties of the electron system is defined and evaluated. The formalism includes the vacuum radiation corrections to the electron system. Expressions for the energy shifts and linewidths induced by the external radiation are obtained.

1. INTRODUCTION

If an electron system, such as that of an atom, is subject to an external electromagnetic radiation, its energy levels are shifted and the linewidths change. We must stress the fact that we are considering here an external radiation different from the electromagnetic radiation of which the electron currents themselves are the source. The latter field we will call the self-field. It gives rise to shifts (e.g., Lamb shift) and the natural linewidth.

The effect of an external radiation on the energy levels of atoms has been investigated by several authors, both theoretically[1-4] and experimentally.[5,6] In this theoretical work one tries to construct a density matrix for the electron system. Sometimes